6

Influence of Nozzle Orifice Geometry and Fuel Properties on Flow and Cavitation Characteristics of a Diesel Injector

Sibendu Som[1], Douglas E. Longman[1],
Anita I. Ramirez[2] and Suresh Aggarwal[2]
[1]*Argonne National Laboratory,*
[2]*University of Illinois at Chicago,*
USA

1. Introduction

Cavitation refers to the formation of bubbles in a liquid flow leading to a two-phase mixture of liquid and vapor/gas, when the local pressure drops below the vapor pressure of the fluid. Fundamentally, the liquid to vapor transition can occur by heating the fluid at a constant pressure, known as boiling, or by decreasing the pressure at a constant temperature, which is known as cavitation. Since vapor density is at least two orders of magnitude smaller than that of liquid, the phase transition is assumed to be an isothermal process. Modern diesel engines are designed to operate at elevated injection pressures corresponding to high injection velocities. The rapid acceleration of fluid in spray nozzles often leads to flow separation and pockets of low static pressure, prompting cavitation. Therefore, in a diesel injector nozzle, high pressure gradients and shear stresses can lead to cavitation, or the formation of bubbles.

Cavitation, in diesel fuel injectors can be beneficial to the development of the fuel spray, since the primary break-up and subsequent atomization of the liquid fuel jet can be enhanced. Primary breakup is believed to occur in the region very close to the nozzle tip as a result of turbulence, aerodynamics, and inherent instability caused by the cavitation patterns inside the injector nozzle orifices. In addition, cavitation increases the liquid velocity at the nozzle exit due to the reduced exit area available for the liquid. Cavitation patterns extend from their starting point around the nozzle orifice inlet to the exit where they influence the formation of the emerging spray. The improved spray development is believed to lead to more complete combustion process, lower fuel consumption, and reduced exhaust gas and particulate emissions. However, cavitation can decrease the flow efficiency (discharge coefficient) due to its affect on the exiting jet. Also, imploding cavitation bubbles inside the orifice can cause material erosion thus decreasing the life and performance of the injector. Clearly an optimum amount of cavitation is desirable and it is important to understand the sources and amount of cavitation for more efficient nozzle designs.

The flow inside the injector is controlled by dynamic factors (injection pressure, needle lift, etc.) and geometrical factors (orifice conicity, hydrogrinding, etc.). The effects of dynamic

factors on the injector flow, spray combustion, and emissions have been investigated by various researchers including (Mulemane, 2004; Som, 2009a, 2010a; Payri, 2009). There have also been experimental studies concerning the effects of nozzle orifice geometry on global injection and spray behavior (Bae, 2002; Blessing, 2003; Benajes, 2004; Han, 2002; Hountalas, 2005; Payri, 2004, 2005, 2008; Som, 2009c). The literature review indicates that while the effect of orifice geometry on the injector flow and spray processes has been examined to some extent, its influence on engine combustion and emissions is not well established (Som, 2010b, 2011). To the best of our knowledge, the influence of nozzle geometry on spray and combustion characteristics has also not been studied numerically, mainly due to the complicated nature of flow processes associated. These form a major motivation for the present study i.e., to examine the effects of nozzle orifice geometry on inner nozzle flow under diesel engine conditions. With increasingly stricter emission regulations and greater demand on fuel economy, the injector perhaps has become the most critical component of modern diesel engines. Consequently, it is important to characterize the effects of orifice geometry on injection, atomization and combustion behavior, especially as the orifice size keeps getting smaller and the injection pressure higher. In order to achieve the proposed objectives, we first examine the effects of orifice geometry on the injector flow, including the cavitation and turbulence generated inside the nozzle.

Biofuels are an important part of our country's plan to develop diverse sources of clean and renewable energy. These alternative fuels can help increase our national fuel security through renewable fuel development while simultaneously reducing emissions from the transportation sector. Biodiesel is a particularly promising biofuel due to its compatibility with the current fuel infrastructure geared toward compression-ignition engines. Using biodiesel as a blending agent can prolong the use of petrodiesel. Biodiesel is also easily produced from domestic renewable resources such as soy, rape-seed, algae, animal fats, and waste oils. Our literature search (Som, 2010b) identified relatively few studies dealing with the injection and spray characteristics of biodiesel fuels. Since there are significant differences in the thermo-transport properties of petrodiesel and biodiesel fuels, the injection and spray characteristics of biodiesel can be expected to differ from those of petrodiesel. For instance, due to differences in vapor pressure, surface tension, and viscosity, the cavitation and turbulence characteristics of biodiesel and diesel fuels inside the injector may be significantly different. The injector flow characteristics determine the boundary conditions at the injector orifice exit, including the rate of injection (ROI) profile as well as the cavitation and turbulence levels; this can have a significant influence on the atomization and spray characteristics, and consequently on engine performance. Som et al. (Som, 2010b) compared the injection and spray characteristics of diesel and biodiesel (from soy-based feedstock) using an integrated modeling approach. This modeling approach accounts for the influence in nozzle flow effects such as cavitation and turbulence (Som, 2010a) on spray-combustion development using the recently developed Kelvin Helmholtz-Aerodynamic Cavitation Turbulence (KH-ACT) primary breakup model (Som, 2009b, 2010c). Another objective of the current study is to demonstrate a framework within which boundary conditions for spray and combustion modeling for different orifice shapes and alternate fuels of interest can be available from high-fidelity nozzle flow simulations.

2. Computational model

The commercial CFD software FLUENT v6.3 was used to perform the numerical simulation of flow inside the nozzle. FLUENT employs a mixture based model as proposed by Singhal

et al. (Singhal, 2002). The two-phase model considers a mixture comprising of liquid fuel, vapor, and a non-condensable gas. While the gas is compressible, the liquid and vapor are considered incompressible. In addition, a no-slip condition between the liquid and vapor phases is assumed. Then the mixture properties are computed by using the Reynolds–Averaged continuity and momentum equations (Som, 2009a).

$$\frac{\partial u_j}{\partial x_j} = 0 \tag{1}$$

$$\rho \frac{\partial u_i u_j}{\partial x_j} = -\frac{\partial P}{\partial x_i} + \frac{\partial \tau_{ij}}{\partial x_j} \tag{2}$$

where $\tau_{ij} = (\mu + \mu_t)\left\{\frac{\partial u_i}{\partial x_j} + \frac{\partial u_j}{\partial x_i}\right\}$, $\mu_t = C_\mu \rho \frac{k^2}{\in}$ is the turbulent viscosity

In order to account for large pressure gradients, the realizable $k-\in$ turbulence model is incorporated along with the non-equilibrium wall functions.

$$\frac{\partial \rho u_j k}{\partial x_j} = \frac{\partial}{\partial x_j}\left[\left(\mu + \frac{\mu_t}{\sigma_k}\right)\frac{\partial k}{\partial x_j}\right] + \text{P-}\rho \in \tag{3}$$

$$\text{where P (production of turbulent kinetic energy)} = \mu_t \frac{\partial u_i}{\partial x_j}\left[\frac{\partial u_i}{\partial x_j} + \frac{\partial u_j}{\partial x_i}\right] - \frac{2}{3}\frac{\partial u_i}{\partial x_i}\left\{\rho k + \mu_t \frac{\partial u_k}{\partial x_k}\right\} \tag{4}$$

$$\frac{\partial \rho u_j \in}{\partial x_j} = \frac{\partial}{\partial x_j}\left[\left(\mu + \frac{\mu_t}{\sigma_k}\right)\frac{\partial \in}{\partial x_j}\right] + \frac{\in}{k}\left[c_1 \text{P-} c_2 \rho \in + c_3 \rho k \frac{\partial u_k}{\partial x_k}\right]$$

The turbulent viscosity is modeled for the whole mixture. The mixture density and viscosity are calculated using the following equations:

$$\rho = \alpha_v \rho_v + (1 - \alpha_v - \alpha_g)\rho_l + \alpha_g \rho_g \tag{5}$$

$$\mu = \alpha_v \mu_v + (1 - \alpha_v - \alpha_g)\mu_l + \alpha_g \mu_g \tag{6}$$

where ρ and μ are the mixture density and viscosity respectively, and the subscripts v, l, g represent the vapor, liquid, and gas respectively. The mass (f) and volume fractions (α) are related as:

$$\alpha_v = f_v \frac{\rho}{\rho_v},\ \alpha_l = f_l \frac{\rho}{\rho_l},\ \text{and}\ \alpha_g = f_g \frac{\rho}{\rho_g} \tag{7}$$

Then the mixture density can be expressed as:

$$\frac{1}{\rho} = \frac{f_v}{\rho_v} + \frac{f_g}{\rho_g} + \frac{1 - f_v - f_g}{\rho_l} \tag{8}$$

The vapor transport equation governing the vapor mass fraction is as follows:

$$\rho \frac{\partial u_j f_v}{\partial x_j} = \frac{\partial}{\partial x_j}\left(\Gamma \frac{\partial f_v}{\partial x_j} \right) + \mathrm{R_e} - \mathrm{R_c} \tag{9}$$

where u_i is the velocity component in a given direction (i=1,2,3), Γ is the effective diffusion coefficient, and $\mathrm{R_e}$, $\mathrm{R_c}$ are the vapor generation and condensation rate terms (Brennen, 1995) computed as:

$$\begin{aligned} \mathrm{R_e} &= \mathrm{C_e} \frac{\sqrt{k}}{\sigma} \rho_l \rho_v \left(1 - f_v - f_g\right) \sqrt{\frac{2\left(P_v - P\right)}{3\rho_l}} \\ \mathrm{R_c} &= \mathrm{C_c} \frac{\sqrt{k}}{\sigma} \rho_l \rho_v f_v \sqrt{\frac{2\left(P - P_v\right)}{3\rho_l}} \end{aligned} \tag{10}$$

where σ and P_v are the surface tension and vapor pressure of the fluid respectively, and k and P are the local turbulent kinetic energy and static pressure respectively. An underlying assumption here is that the phenomenon of cavitation inception (bubble creation) is the same as that of bubble condensation or collapse. Turbulence induced pressure fluctuations are accounted for by changing the phase-change threshold pressure at a specified temperature ($\mathrm{P_{sat}}$) as:

$$P_v = P_{sat} + {}^{P_{turb}}\!/_{2} \text{ where, } P_{turb} = 0.39\rho k \tag{11}$$

The source and sink terms in equation (10) are obtained from the simplified solution of the Rayleigh-Plesset equation (Brennen, 1995). No-slip boundary conditions at the walls and symmetry boundary condition at the center line are employed for the HEUI 315-B injector simulations (cf. Figure 3a).

3. Results and discussion

This section will first present a new improved criterion for cavitation inception for production injector nozzles. This new criterion will provide a tool for assessing cavitation under turbulent regimes typical in diesel injector nozzles. The influence of nozzle orifice geometry on in-nozzle flow development will be presented next. The influence of fuel properties such as density, viscosity, surface tension, and vapor pressure on nozzle flow characteristics will be presented. Cavitation and turbulence generated inside the nozzle due to geometry and fuel changes will also be quantified.

3.1 An Improved criterion for cavitation inception

According to the traditional criterion, cavitation occurs when the local pressure drops below the vapor pressure of the fuel at a given temperature i.e., when $-p + p_v > 0$. This criterion can be represented in terms of a cavitation index (K) as:

$$K_{Classical} = \frac{p - p_b}{p_b - p_v} < -1 \Rightarrow Cavitating \tag{12}$$

where p , p_b , p_v are the local pressure, back pressure, and vapor pressure, respectively. This criterion has been extensively used in the cavitation modeling community. However, Winer and Bair (Winer, 1987) and Joseph (Joseph, 1998) independently proposed that the important parameter for cavitation is the total stress that includes both the pressure and normal viscous stress. This was consistent with the cavitation experiments in creeping shear flow reported by Kottke et al. (Kottke, 2005), who observed the appearance of cavitation bubbles at pressures much higher than vapor pressure. Following an approach proposed by Joseph (Joseph, 1998) and Dabiri et al. (Dabiri, 2007), a new criterion based on the principal stresses was derived and implemented. The formulation for the new criterion is summarized below.

Maximum tension criterion: $-p - 2\mu S_{11} + p_v > 0$

Minimum tension criterion: $-p + 2\mu S_{11} + p_v > 0$

The new criteria can be expressed in terms of the modified cavitation index as:

$$K_{\max} = \frac{p + 2\mu S_{11} - p_b}{p_b - p_v} < -1 \Rightarrow Cavitating \tag{13}$$

$$K_{\min} = \frac{p - 2\mu S_{11} - p_b}{p_b - p_v} < -1 \Rightarrow Cavitating \tag{14}$$

where the strain rate S_{11} is computed as:

$$S_{11} = \sqrt{\left(\frac{\partial u}{\partial x}\right)^2 + \left(\frac{\partial u}{\partial y} + \frac{\partial v}{\partial x}\right)^2} \tag{15}$$

where u, v are the velocities in x, y direction respectively.

Under realistic Diesel engine conditions where flow inside the nozzle is turbulent, turbulent stresses prevail over laminar stresses. Accounting for the effect of turbulent viscosity the new criteria is further modified as:

$$K_{\text{max-turb}} = \frac{p + 2(\mu + \mu_t)S_{11} - p_b}{p_b - p_v} < -1 \Rightarrow Cavitating \tag{16}$$

$$K_{\text{min-turb}} = \frac{p - 2(\mu + \mu_t)S_{11} - p_b}{p_b - p_v} < -1 \Rightarrow Cavitating \tag{17}$$

The experimental data from Winklhofer et al. (Winklhofer, 2001) was used for a comprehensive model validation. These experiments were conducted in a transparent, quasi-2-D geometry wherein the back pressure was varied to achieve different mass flow rates. To the best of our knowledge this experimental data-set is most comprehensive in terms of two phase information and inner nozzle flow properties.

Figure 1 presents the measured cavitation contour at injection and back pressures of 100 and 40 bar respectively, owing to a Reynolds number of 16,000 approximately. It is clearly seen from the marked red line that there is significant amount of cavitation at the orifice inlet. These cavitation contours extend to certain distance inside the orifice. The vapor fraction

contour shows no cavitation (blue represents pure liquid). The classical criterion which basically is another way of representing the predicted vapor fraction contour also captures the same trend, i.e., hardly any cavitation is observed. The laminar criteria shows cavitation inception, however, no advection of the fuel vapor into the orifice is observed. The turbulent criteria seems to capture more cavitation with C_t =2 agreeing better with experimental data that all the other criteria.

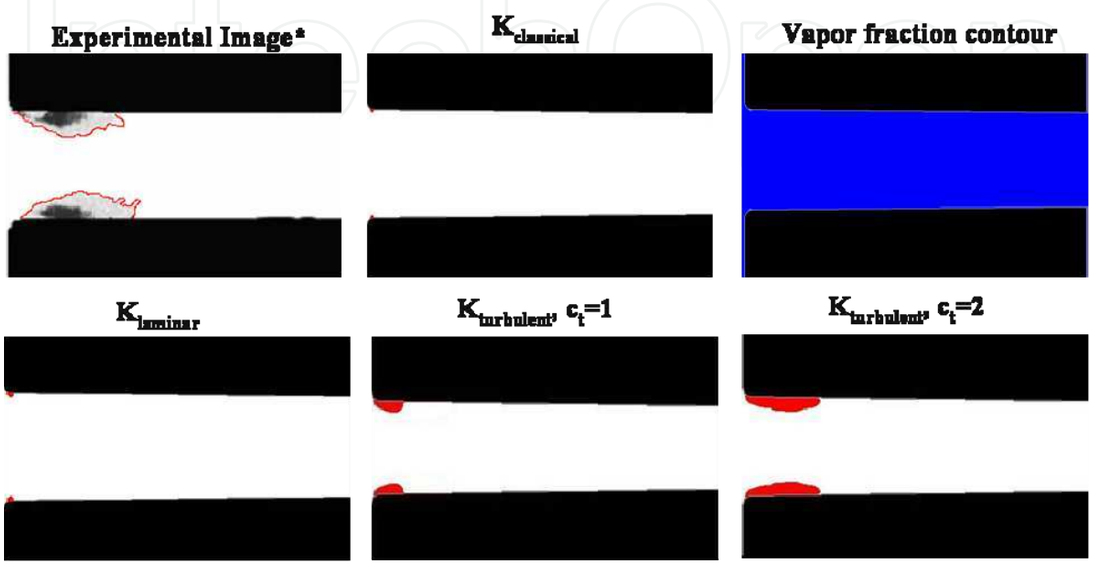

Fig. 1. Comparison between the measured (Winklhofer, 2001), predicted vapor fraction contours, and cavitation inception regions predicted by different cavitation criteria. The injection and back pressures are 100bar and 40bar respectively.

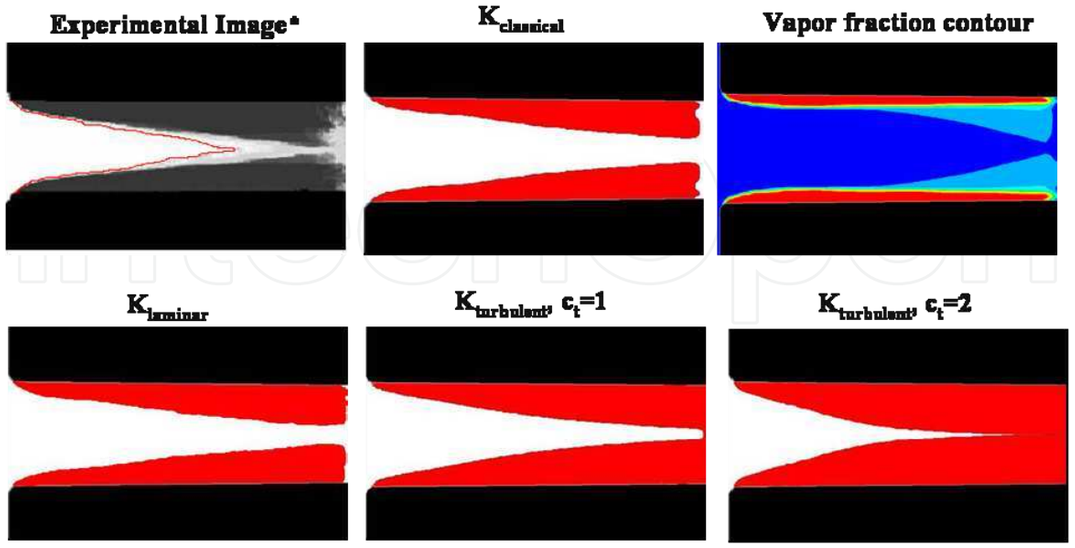

Fig. 2. Comparison between the measured (Winklhofer, 2001), predicted vapor fraction contours, and cavitation inception regions predicted by different cavitation criteria. The injection and back pressures are 100bar and 20bar respectively.

Figure 2 presents the measured cavitation contour at injection and back pressures of 100 and 20 bar respectively, owing to a Reynolds number of 18,000 approximately. It is clearly seen from the marked red line in the experimental image (Winklhofer, 2001) that there is a significant amount of cavitation at the top and bottom of orifice inlet. These cavitation contours are symmetric in nature and are advected by the flow to reach the nozzle orifice exit.

The cavitation contours join near the orifice exit thus the exit is completely covered by fuel vapor. The predicted vapor fraction contour also shows significant amount of cavitation represented by the fuel vapor contour (in red). However, there is still a significant amount of liquid fuel (in blue) present at the orifice exit and the vapor fraction contours do not join together as was the case in experiments. The classical criterion which basically is another way of representing the predicted vapor fraction also captures the trend as the vapor fraction contour. The laminar criterion predicts marginal improvement to the classical criterion. This is expected since for high Reynolds number flows the difference between these criteria was observed to diminish (Padrino, 2007). Increase in Reynolds number results in an increase in turbulence levels inside the orifice. Thus the turbulent stress criterion is seen to improve the predictions of vapor fraction contours significantly. All the experimentally observed characteristics are captured by the turbulent stress criterion i.e., the vapor contours from top and bottom of the orifice are seen to merge together resulting in pure vapor at orifice exit. The turbulent criterion seems to capture more cavitation with C_t =2 agreeing better with experimental data than all the other criteria.

The simulations using the new cavitation criterion show significant improvement in prediction of cavitation contours especially in the turbulent regime under realistic injection conditions. Future studies will focus on performing such studies in realistic geometries of interest characteristerized by three dimensional flow features. Winklhofer et al. (Winklhofer, 2001) experiments, although performed under realistic injection conditions, do not capture the 3D effects which are essential to flow development.

3.2 Effect of nozzle orifice geometry on inner nozzle flow development

This section will focus on capturing the influence of nozzle orifice geometry on in-nozzle flow development such as cavitation and turbulence in addition to flow variables such as velocity, discharge coefficient etc. The base nozzle orifice geometry which is cylindrical and non-hydroground will be presented first. The single orifice simulated for the full-production, mini-sac nozzle used in the present study is shown in Figure 3. The nozzle has six cylindrical holes with diameter of 169 µm at an included angle of 126°. The discharge coefficient (C_d), velocity coefficient (C_v) and area contraction coefficient (C_a), used to characterize the nozzle flow, are described below. The discharge coefficient (C_d) is calculated from:

$$C_d = \frac{\dot{M}_{actual}}{\dot{M}_{th}} = \frac{\dot{M}_{actual}}{A_{th}\sqrt{2 * \rho_f * \Delta P}} \tag{18}$$

where $\dot{M}_{actual}$ is the mass flow rate measured by the rate of injection (ROI) meter (Bosch, 1966), or calculated from FLUENT simulations, A_{th} is the nozzle exit area, and $\dot{M}_{th}$ is the theoretical mass flow rate. The three coefficients are related as (Naber , 1996):

$$C_d = C_v * C_a \tag{19}$$

Here the area contraction coefficient is defined as:

$$C_a = \frac{A_{effective}}{A_{th}} \tag{20}$$

where $A_{effective}$ represents the area occupied by the liquid fuel. C_a is an important parameter to characterize cavitation, as it is directly influenced by the amount of vapor present at the nozzle exit. The Reynolds number is calculated from:

$$\mathrm{Re} = \frac{V_{th} D_{th} \rho_{fuel}}{\mu_{fuel}} \tag{21}$$

where D_{th} is the nozzle exit diameter.

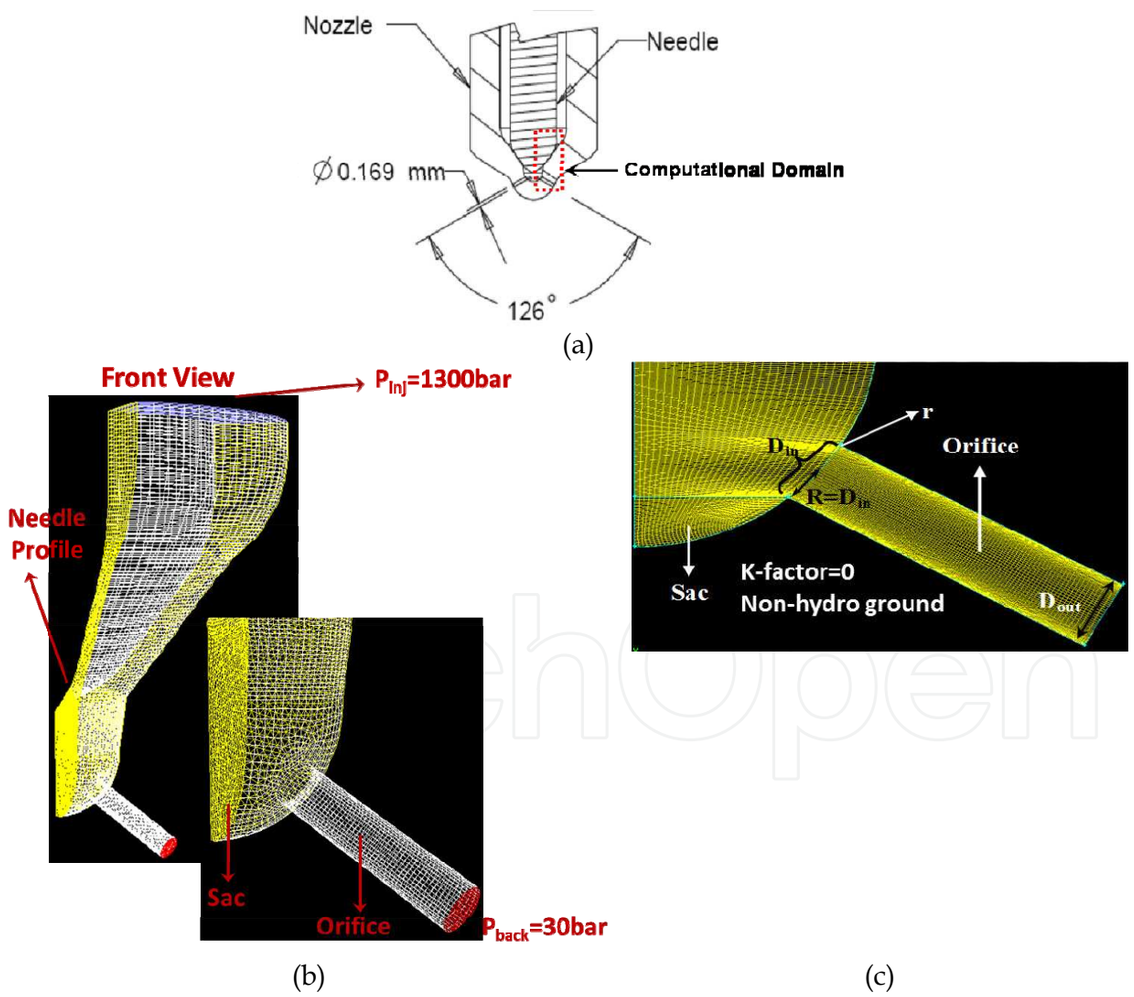

Fig. 3. (a) Injector nozzle geometry along with the computational domain. (b) The 3-D grid generated, specifically zooming in on the sac and orifice regions. (c) Zoomed 2-D view of the orifice and sac regions.

The influence of nozzle orifice geometry is characterized by comparing the in-nozzle flow characteristics of the base nozzle against a hydroground nozzle. The hydroground nozzle has the same nominal dimensions as the base nozzle except the hydrogrounding resulting in a small inlet radius of curvature. The essential features of the nozzle orifices simulated are shown in Table 1.

Geometrical Characteristics	Base Nozzle	Hydroground Nozzle
D_{in} (μm)	169	169
D_{out} (μm)	169	169
K_{factor}	0	0
r/R	0	0.014
L/D	4.2	4.2

Table 1. Geometrical Characteristics of nozzle orifice simulated.

Figure 4 presents vapor fraction contours for the base and hydroground nozzles at P_{in}=1300bar, P_b=30bar, and full needle open position. Simulations were performed for diesel fuel (properties shown in Table 2). The 3D view of the cavitation contours shows that vapor generation only occurs at the orifice inlet for both the orifices. For the base nozzle these cavitation contours are advected by the flow to reach the orifice exit. Consequently, the computed area coefficient (C_a) was found to be 0.96 for this case. A smoother orifice inlet (i.e., r/R=0.014) clearly leads to a decrease in cavitation. The small amount of vapor generated is restricted to the nozzle inlet. Thus chamfering/rounding the orifice inlet geometry can inhibit cavitation by allowing a smoother entry to the orifice, and also improve the nozzle flow efficiency (C_d) as discussed below. This is due to the fact that flow uniformity in the orifice entrance region is significantly enhanced for the hydroground nozzle hence, cavitation is almost completely inhibited. This observation is consistent with those reported by other researchers. A 2D cut-plane was constructed passing though the mid-plane. This view also highlights the fact that the hydroground nozzle cavitates significantly less compared to the base nozzle.

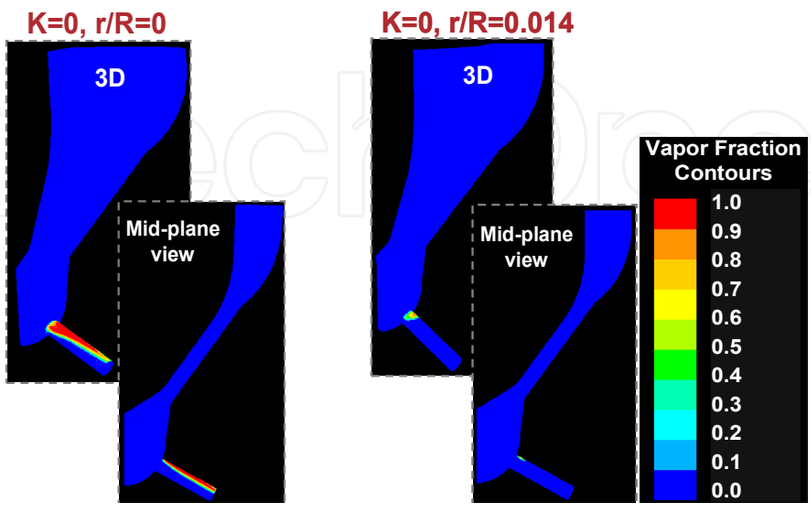

Fig. 4. 3D and mid-plane views of vapor fraction contours for the base and hydroground nozzles. Simulations were performed at P_{in}=1300bar, P_b=30bar, and full needle open position.

Figure 5 presents the velocity vectors plotted at the orifice inlet of the mid-plane for the base and hydroground nozzles presented in the context of previous figure. The zoomed view clearly shows that the velocity vectors point away from the wall for the base nozzle, while they are aligned with the flow for the hydroground nozzle thus ensuring a smooth entry into the orifice which decreases cavitation. As mentioned earlier, difference in cavitation characteristics plays a central role in spray breakup processes. Hence, spray behavior of a hydroground nozzle is expected to be different from that of the base nozzle.

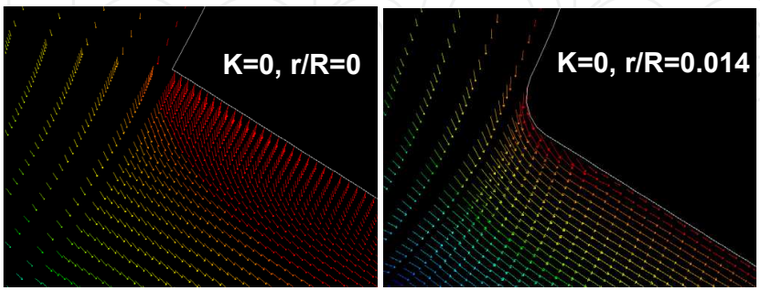

Fig. 5. Velocity vectors shown at the orifice inlet of the mid-plane for base and cylindrical nozzles presented in the context of Fig. 4.

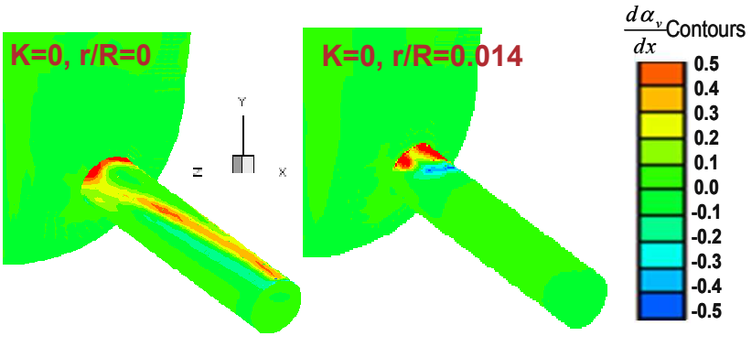

Fig. 6. Contours of $\frac{d\alpha_v}{dx}$ for the two injector orifices described in the context of Fig. 4.

Figure 6 presents the contours of $\frac{d\alpha_v}{dx}$ where α_v is the fuel vapor fraction and 'x' is the coordinate axis along the orifice. Hence the parameter $\frac{d\alpha_v}{dx}$ represents the production or consumption of fuel vapor inside the orifice. Positive represents production while negative values indicate consumption of fuel vapor. A value of 0 represents no change in the fuel vapor fraction with axial position. A zoomed 3D view of the sac and upper orifice region is shown. For both the nozzles, the sac region is composed of pure liquid hence $\frac{d\alpha_v}{dx} = 0$. Since the vapor generation takes place at the upper side of orifice inlet it is not surprising that $\frac{d\alpha_v}{dx}$ is positive. The vapor fraction contours for the base nozzle showed pure vapor existence throughout the upper part of orifice (cf. Fig. 4). However, $\frac{d\alpha_v}{dx}$ only predicts

pockets of vapor formation indicating that the remaining vapor is due to advection from the orifice inlet. In the case of conical (not shown here) and hydroground nozzles, vapor is generated at the orifice inlet however it is completely consumed soon after; hence the exit of the orifice is composed of pure liquid fuel only.

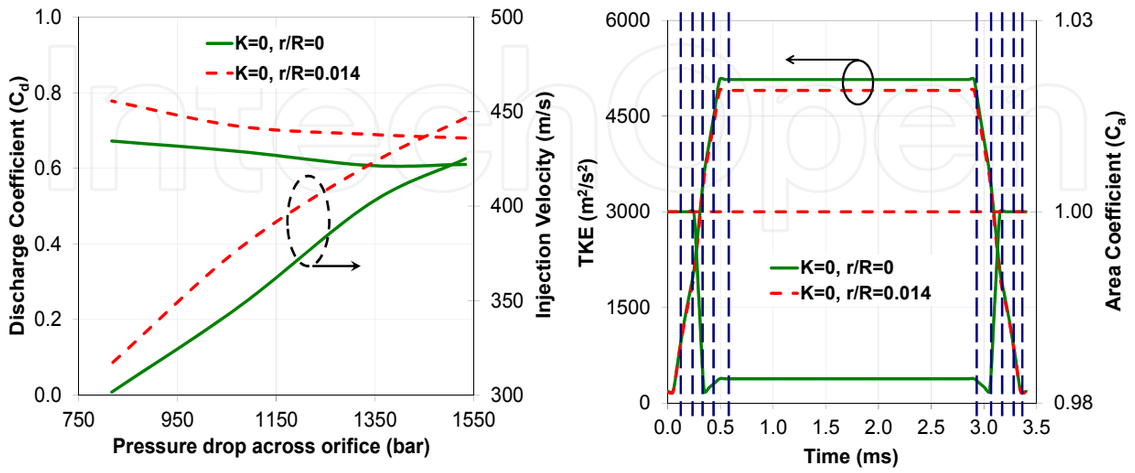

Fig. 7. (a) Discharge coefficient and injection velocity plotted versus pressure drop across the orifice, (b) Turbulence parameters such as TKE and TDR as a function of time for the base and hydrogroud nozzles shown in Figure 4.

Figure 7a presents C_d and injection velocity at nozzle exit for different pressure drops across the orifice. The back pressure was always fixed at 30bar, hence, the change in injection pressure resulted in change in pressure drop across the orifice. The methodology for calculating these parameters was discussed earlier. With increase in injection pressure, injection velocity at the orifice exit is seen to increase, which is expected. It should be noted that the injection velocity reported is an average value across the orifice. As expected, the average injection velocity and discharge coefficient is lower for the base nozzle owing to the presence of cavitation at the orifice exit. The influence of nozzle geometry on turbulence levels at the nozzle orifice exit is investigated in Fig. 7b since these parameters are directly input in spray simulations as rate profiles for cavitation, turbulence, and fuel mass injected. The different needle lift positions simulated are also shown. The peak needle lift of this injector was 0.275 mm which corresponds to full needle open position. Other needle positions simulated are: 0.05mm, 0.1mm, 0.15mm, and 0.2mm open respectively. A general trend observed is that the turbulent kinetic energy (TKE) increased with needle lift position which is expected since the injection pressure also increased resulting in higher Reynolds numbers. TKE and turbulent dissipation rate (TDR) were seen to be higher for the base nozzle case at all needle lift positions. Turbulence is known to play a key role in spray breakup processes; hence, accounting for such differences in turbulence levels between orifices is expected to improve spray predictions. The reason for similar turbulence levels at lower needle lifts is due to the fact that at low needle lift positions, the area between the needle and orifice governs the fluid dynamics inside the nozzle. However, at full needle lift position during the quasi-steady injection period, the orifice plays a critical role in the flow development inside the nozzle. Area coefficient was unity for the hydroground nozzle

which is expected since this orifice inhibits cavitation inception completely. These rate profiles are input for the spray simulations (Som, 2009a, 2010b, 2011).

3.3 Influence of fuel properties on nozzle flow

This section presents the influence of fuel properties on nozzle flow development. As mentioned earlier, the nozzle flow characteristics of biodiesel is compared against that of diesel fuel since biodiesel is a lucrative blending agent. Table 2 presents the physical properties of diesel and biodiesel (soy-methyl ester) fuels. There are small differences in density and surface tension between these fuels. However, major differences are observed in viscosity and vapor pressure values. These differences are expected to influence the nozzle flow and spray development.

Fuel Property	Diesel	Biodiesel
Carbon Content [wt %]	87	76.74
Hydrogen Content [wt %]	13	12.01
Oxygen Content [wt %]	0	11.25
Density @ 15^{o}C (kg/m^{3})	822.7	877.2
Dynamic Viscosity @ 40^{o}C (cP)	1.69	5.626
Surface Tension @ 25^{o}C (N/m)	0.0020	0.00296
Vapor Pressure @ 25^{o}C (Pa)	1000	1

Table 2. Comparison of physical properties of diesel and biodiesel (soy-methyl ester) fuels

Figure 8 presents the vapor fraction contours for diesel and biodiesel for P_{inj}=1300 bar and P_{back}=30 bar. The 3-D view of the cavitation contours indicates that vapor generation occurs at the orifice inlet for both the fuels. For diesel, these cavitation contours, generated at the upper side of the orifice, reach the orifice exit. In contrast, for biodiesel, the cavitation contours only extend a few microns into the orifice and do not reach the injector exit. Since cavitation plays a significant role in primary breakup, the atomization and spray behavior of these fuels is expected to be different. The mid-plane view also indicates that the amount of cavitation is significantly reduced for biodiesel compared to diesel. This is mainly due to two reasons:

1. The vapor pressure of biodiesel is lower than diesel fuel. Cavitation occurs when the local pressure is lower than the vapor pressure of the fuel. Hence, reduction in vapor formation can be expected for fuels with lower vapor pressures. Although injection pressures are very high, the differences in vapor pressure values are also important for cavitation inception.
2. The viscosity of biodiesel is higher compared to diesel fuel (cf. Table 2). This increased viscosity results in lower velocities inside the sac and orifice, which in turn decreases the velocity gradients. This also results in lowering of cavitation patterns for biodiesel.

Figure 9 presents contours of the magnitude of velocity at the mid-plane and orifice exit plane for diesel and biodiesel fuels for the case presented in Fig. 8. The flow entering the orifice encounters a sharp bend (i.e., large velocity and pressure gradients) at the upper side of the orifice inlet, causing cavitation in this region, as indicated by the vapor fraction contours. Upstream of the orifice, the velocity distribution appears to be similar for the two fuels. However, at the orifice exit, the contours indicate regions of higher velocity for diesel compared to biodiesel. This is related to the fact that the viscosity (cf. Table 2) of biodiesel is

higher than that of diesel fuel. The velocity contours at the orifice exit indicate fairly symmetrical distribution with respect to the y-axis for both fuels.

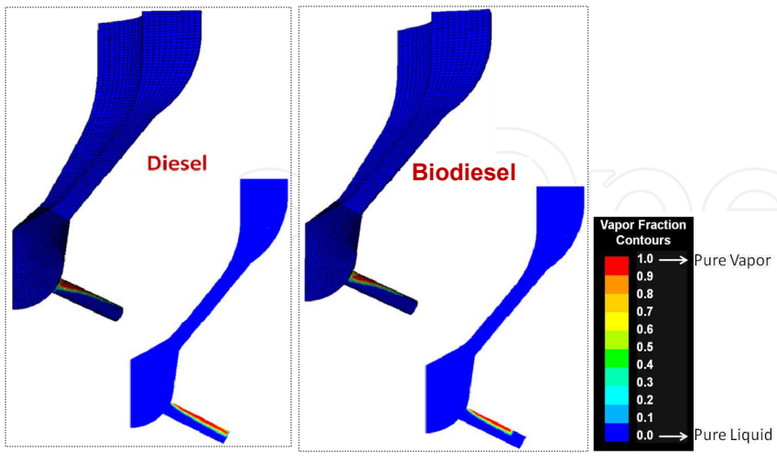

Fig. 8. Vapor fraction contours for diesel and biodiesel inside the injector and at the mid-plane. The simulations were performed at full needle open position with P_{inj} = 1300 bar and P_{back} = 30 bar.

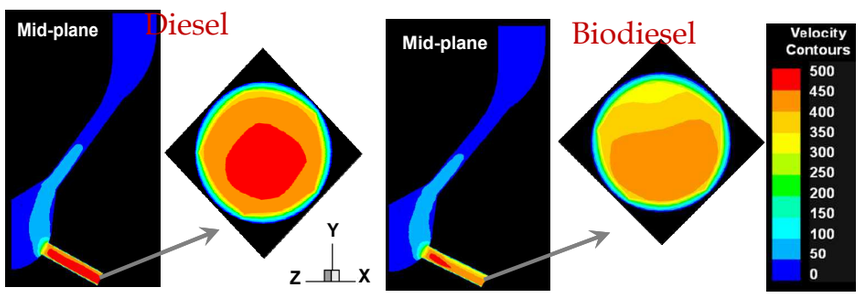

Fig. 9. Velocity contours for diesel and biodiesel at the mid-plane and orifice exit. The simulations were performed at full needle open position with P_{inj} = 1300 bar and P_{back} = 30 bar.

Figure 10 presents the computed fuel injection velocity, mass flow rate, C_d, and normalized TKE at the nozzle exit for different injection pressures. All these parameters are obtained by computing the 3-D flow inside the injector and then averaging the properties at the orifice exit. As expected, with increased injection pressure, the injection velocity and mass flow rate at the orifice exit increase (cf. Fig. 10a). However, the injection velocity, mass flow rate, and discharge coefficient are lower for biodiesel compared to diesel fuel. This difference in injection velocity and hence in mass flow rate can be attributed to the significantly higher viscosity of biodiesel. The lower mass flow rate for biodiesel implies that, for a fixed injection duration, a lesser amount of biodiesel will be injected into the combustion chamber compared to diesel. Combined with the lower heating value of biodiesel, this would lead to lower engine output with biodiesel compared to diesel fuel. As indicated in Fig. 10b, the average TKE at the nozzle exit is also lower for biodiesel. This is due to the fact that the Reynolds number is lower for biodiesel due to its higher effective viscosity. This has implications for the atomization and spray characteristics of the two fuels, since the turbulence level at the orifice exit influences the primary breakup.

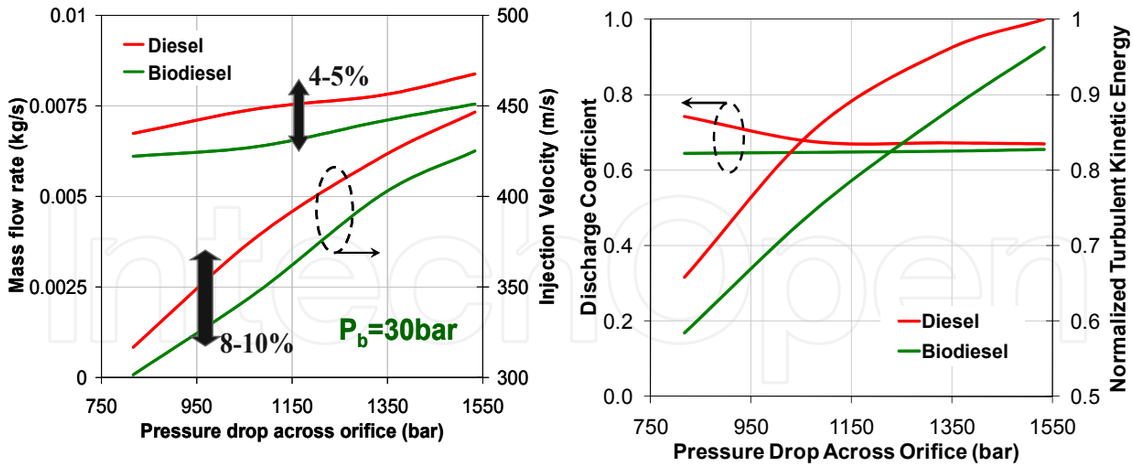

(a) (b)

Fig. 10. Computed flow properties at the nozzle exit versus pressure drop in the injector for diesel and biodiesel fuels: (a) mass flow rate and injection velocity; (b) discharge coefficient and normalized TKE.

4. Conclusion

The flow inside the nozzle is critical in spray, combustion, and emission processes for an internal combustion engine. Inner nozzle flows are multi-scale and multi-phase in nature, hence, challenging to capture both in experiments and simulations. Cavitation and turbulence generated inside the nozzle is known to influence the primary breakup of the fuel, especially in the near nozzle region. The authors capture the in-nozzle flow development using the two-phase flow model in FLUENT software. The influence of definition of cavitation inception is first analyzed by implementing an improved criterion for cavitation inception under turbulent conditions. While noticeable differences between the standard and advanced criteria for cavitation inception are observed under two-dimensional flow conditions, thorough development and validation is necessary before implementing in real injection flow simulations.

Since the injector nozzle is a critical component of modern internal combustion engines, the influence of orifice geometry and fuel properties on in-nozzle flow development were also characterized. Both cavitation and turbulence was reduced using a hydroground nozzle compared to a base production nozzle. This will result in significant differences in spray, combustion, and emission behaviour also for these nozzles. Biodiesel being a lucrative blending agent for compression ignition engine applications was then compared to diesel fuel for inner nozzle flow development. Cavitation and turbulence generated inside the nozzle was observed to be lower for biodiesel compared to diesel fuel. Additionally, boundary conditions in terms of cavitation, turbulence, and flow variables were obtained for spray combustion simulations as a function of time for the detailed nozzle flow simulations.

5. Acknowledgment

The submitted manuscript has been created by UChicago Argonne, LLC, Operator of Argonne National Laboratory ("Argonne"). Argonne, a U.S. Department of Energy Office of Science

laboratory, is operated under Contract No. DE-AC02-06CH11357. The U.S. Government retains for itself, and others acting on its behalf, a paid-up nonexclusive, irrevocable worldwide license in said article to reproduce, prepare derivative works, distribute copies to the public, and perform publicly and display publicly, by or on behalf of the Government.

6. References

Bae C., Yu J., Kang J., Kong J., Lee K.O. 2002. Effect of nozzle geometry on the common-rail diesel spray. *SAE Paper No*. 2002-01-1625.

Benajes, J., Pastor, J.V., Payri, R., Plazas, A.H. 2004. Analysis of the influence of diesel nozzle geometry in the injection rate characteristics. *Journal of Fluids Engineering*, 126, 63-71.

Blessing, M., Konig, G., Kruger, C., Michels, U., Schwarz, V. 2003. Analysis of flow and cavitation phenomena in diesel injection nozzles and its effects on spray and mixture formation. *SAE Paper No*. 2003-01-1358.

Bosch, W. 1966. The Fuel Rate Indicator: A New Measuring Instrument for Display of the Characteristics of Individual Injection. *SAE Paper No*. 660749.

Brennen, E.C. 1995. Cavitation and Bubble Dynamics. Oxford University Press.

Dabiri, S., Sirignano, W.A., Joseph, D.D. 2007. Cavitation in an Orifice Flow. *Physics of Fluids*, 19, pp. 072112-1-072112-9.

Han, J.S., Lu, P.H., Xie, X.B., Lai, M.C., Henein, N.A. 2002. Investigation of diesel spray primary breakup and development for different nozzle geometries. *SAE Paper No*. 2002-01-2775.

Hountalas, D.T., Zannis, T.C., Mavropoulos, G.C., Schwarz, V., Benajes, J., Gonzalez C.A. 2005. Use of a Multi-Zone Combustion Model to Interpret the effet of injector nozzle hole geometry on HD DI Diesel Engine performance and pollutant emissions. *SAE Paper No*. 2005-01-0367.

Joseph, D.D. 1998. Cavitation and the state of stress in a flowing liquid. *Journal of Fluid Mechanics*, 366, 367-378.

Kottke, P.A., Bair, S.S., Winer, W.O. 2005. Cavitation in creeping shear flows. *AICHE Journal*, 51, 2150.

Mulemane, A., Han, J.S., Lu, P.H., Yoon, S.J., Lai, M.C. 2004. Modeling dynamic behavior of diesel fuel injection systems. *SAE Paper No*. 2004-01-0536.

Naber, J.D., Siebers, D.L. 1996. Effects of Gas Density and Vaporization on Penetration and Dispersion of Diesel Sprays. *SAE Paper No*. 960034.

Padrino, J.C., Joseph, D.D., Funada, T., Wang, J., and Sirignano, W.A. 2007. Stress-Induced cavitation for the streaming motion of a viscous liquid past a sphere. *Journal of Fluid Mechanics*, 578, 381-411.

Payri, F., Bermudez, V., Payri, R., Salvador, F.J. 2004. The influence of cavitation on the internal flow and the spray characteristics in diesel injection nozzles. *Fuel*, 83, 419-431.

Payri, R., Garcia, J.M., Salvador, F.J., Gimeno, J. 2005. Using spray momentum flux measurements to understand the influence of diesel nozzle geometry on spray characteristics. *Fuel*, 84, 551-561.

Payri, R., Salvador, F.J., Gimeno, J., Zapata, L.D. 2008. Diesel nozzle geometry influence on spray liquid-phase fuel penetration in evaporative conditions. *Fuel*, 87, 1165-1176.

Payri, F., Margot, X., Patouna, S., Ravet, F., Funk, M. 2009. A CFD study of the effect of the needle movement on the cavitation pattern of diesel injectors. *SAE Paper No*. 2009-24-0025.

Singhal, A.K., Athavale, A.K., Li, H., Jiang, Y. 2002. Mathematical basis and validation of the full cavitation model. *Journal of Fluid Engineering*, 124, 617-624.

Som, S. Development and validation of spray models for investigating Diesel engine combustion and emissions. *PhD thesis*, University of Illinois at Chicago; 2009.

Som, S., Ramirez, A.I., Aggarwal, S.K., Kastengren, A.L., El-Hannouny, E.M., Longman, D.E., Powell, C.F., Senecal, P.K. 2009. Development and Validation of a Primary Breakup Model for Diesel Engine Applications. *SAE Paper No*. 2009-01-0838.

Som, S., Aggarwal, S.K. 2009. An Assessment of Atomization Models for Diesel Engine Simulations. *Atomization and Sprays*, 19(9), 885-903.

Som, S., Aggarwal, S.K., El-Hannouny, E.M., Longman, D.E. 2010. Investigation of nozzle flow and cavitation characteristics in a diesel injector. *Journal of Engineering for Gas Turbine and Power*, 132, 1-12.

Som, S., Longman, D.E., Ramírez, A.I., Aggarwal, S.K. 2010. A comparison of injector flow and spray characteristics of biodiesel with petrodiesel. *Fuel*, 89, 4014-4024.

Som, S., Aggarwal, S.K. 2010. Effects of primary breakup modeling on spray and combustion characteristics of compression ignition engines. *Combustion and Flame*, 157, 1179-1193.

Som, S., Ramirez, A.I., Longman, D.E., Aggarwal, S.K. 2011. Effect of nozzle orifice geometry on spray, combustion, and emission characteristics under diesel engine conditions. *Fuel*, 90, 1267-1276.

Winer, W.O., Bair, S. 1987. The Influence of Ambient Pressure on the Apparent Shear Thinning of Liquid Lubricants - An Overlooked Phenomenon. *Proc. Inst. Mech. Eng*., C190-87, pp. 395-398.

Winklhofer, E., Kull, E., Kelz, E., and Morozov, A. 2001. Comprehensive Hydraulic and flow field documentation in model throttle experiments under cavitation conditions. *ILASS Europe*, 2001.

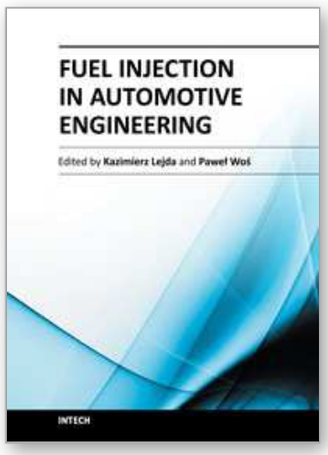

Fuel Injection in Automotive Engineering

Edited by Prof Kazimierz Lejda

ISBN 978-953-51-0528-2
Hard cover, 144 pages
Publisher InTech
Published online 20, April, 2012
Published in print edition April, 2012

The main topic of "Fuel injection in automotive engineering" book is fundamental process that determines the development of internal combustion engines and performances of automotive vehicles. The book collects original works focused on up-to-date issues relevant to improving injection phenomena per se and injection systems as the engine key components.

How to reference

In order to correctly reference this scholarly work, feel free to copy and paste the following:

Sibendu Som, Douglas E. Longman, Anita I. Ramirez and Suresh Aggarwal (2012). Influence of Nozzle Orifice Geometry and Fuel Properties on Flow and Cavitation Characteristics of a Diesel Injector, Fuel Injection in Automotive Engineering, Prof Kazimierz Lejda (Ed.), ISBN: 978-953-51-0528-2, InTech, Available from: http://www.intechopen.com/books/fuel-injection-in-automotive-engineering/influence-of-nozzle-orifice-geometry-and-fuel-properties-on-flow-and-cavitation-characteristics-of-a

INTECH
open science | open minds

InTech Europe
University Campus STeP Ri
Slavka Krautzeka 83/A
51000 Rijeka, Croatia
Phone: +385 (51) 770 447
Fax: +385 (51) 686 166
www.intechopen.com

InTech China
Unit 405, Office Block, Hotel Equatorial Shanghai
No.65, Yan An Road (West), Shanghai, 200040, China
中国上海市延安西路65号上海国际贵都大饭店办公楼405单元
Phone: +86-21-62489820
Fax: +86-21-62489821

IntechOpen